ACS APPLIED MATERIALS & INTERFACES

Research Article

www.acsami.org

Transparent, Conducting ATO Thin Films by Epoxide-Initiated Sol–Gel Chemistry: A Highly Versatile Route to Mixed-Metal Oxide Films

Matthias M. Koebel,*[,†] Digambar Y. Nadargi,[†] Giselle Jimenez-Cadena,[‡] and Yaroslav E. Romanyuk[‡]

[†]Laboratory for Building Science and Technology and [‡]Laboratory for Thin Films and Photovoltaics, Empa, Swiss Federal Laboratories for Materials Science and Technology, Duebendorf 8600, Switzerland

ABSTRACT: A robust synthesis approach to transparent conducting oxide (TCO) materials using epoxide assisted sol–gel chemistry is reported. The new route utilizes simple tin and antimony chloride precursors in aqueous solution, thus eliminating the need for organometallic precursors. Propylene oxide acts as a proton scavenger and drives metal hydroxide formation and subsequent polycondensation reactions. Thin films of antimony-doped tin oxide (ATO) were prepared by dip-coating of mixed metal oxide sols. After annealing at 600 °C in air, structural, electrical and optical properties of undoped and Sb-doped tin oxide films were characterized. Single layer films with 5 mol % Sb doping exhibited an optical transparency which was virtually identical to that of the plain glass substrate and an electrical resistivity of 2.8×10^{-2} Ω cm. SEM and AFM analysis confirmed the presence of surface defects and cracks which increased with increasing Sb dopant concentration. Multiple depositions of identical ATO films showed a roughly 1 order of magnitude decrease in the film resistivity after the third layer, with typical values below 5×10^{-3} Ω cm. This suggests that a second and third deposition fill up residual cracks and defects in the first layer and thus brings out the full performance of the ATO material. The epoxide-assisted sol chemistry is a promising technique for the preparation of mixed oxide thin film materials. Its superiority over conventional alkoxide and metal salt-based methods is explained in the context of a general description of the reaction mechanism.

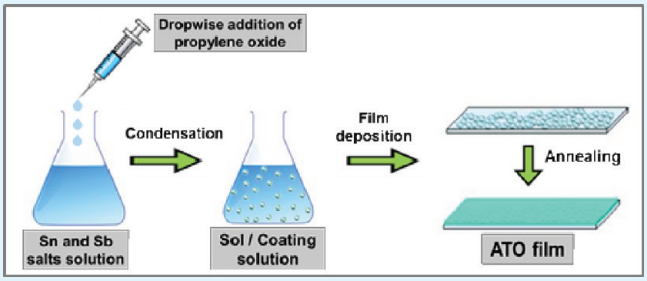

KEYWORDS: *epoxide assisted gelation, liquid chemistry, sol–gel process, dip coating, transparent conducting oxide*

INTRODUCTION

Transparent conducting oxides (TCO) have attracted broad interest for their wide range of applications in optoelectronic devices, sensors, solar cells, and functional coatings.[1−4] The rapid growth of photovoltaic technology and commercialization worldwide has created a need for TCO materials with improved performance or with comparable performance at significantly lower cost. For this reason, sol–gel-based synthesis strategies of metal oxide materials for TCOs have received an increasing amount of attention from the scientific community over the past decade. Advantages of liquid chemistry based synthesis strategies of metal oxide materials are the inherent simplicity and scalability of solution phase chemistry and simple deposition processes. Such methods also allow for a facile up-scaling toward large area applications by means of suitable coating or printing processes.

Standard sol–gel preparation techniques for TCO materials most commonly employ metal alkoxide precursors, which undergo catalyzed hydrolysis and condensation reactions, resulting in a sol of metal oxide particles with nanoscale dimensions (1–100 nm).[5−7] The deposition of such a sol onto a suitable substrate then produces a metal oxide thin film when dried and sintered. However, in many cases alkoxide based sol–gel methods, TCOs are not ideal for the preparation of mixed oxide materials due to often vastly dissimilar hydrolysis rates of the different metal alkoxide precursors. In addition, some metal alkoxides are not commonly available, thus restricting the range of mixed oxides which are accessible and increasing the overall cost.

In principle, the use of nonalkoxide precursors in the sol–gel synthesis of TCOs should be more promising: Recently, Gash and co-workers have reported an alkoxide-free sol–gel synthesis method for preparing various transition, main group and rare earth metal oxides.[8−10] The process, commonly termed epoxide-initiated gelation, utilizes an organic epoxide, which acts as a proton scavenger, driving hydroxide formation and condensation of hydrated metal ions. The epoxide is first protonated and then consumed through an irreversible ring-opening reaction. This is explained in more detail in the Discussion section. Typically, a slow and uniform increase in the pH of the liquid solution is observed, indicating the progress of the reaction and eventually leading to the formation of a metal oxide sol or even an extended metal oxide network structure (a gel). Although primarily used for the preparation of gels and aerogels, this methodology offers perhaps even greater promise for the synthesis of a wide range of metal oxide

Received: January 25, 2012
Accepted: April 2, 2012
Published: April 18, 2012

nanocomposite thin films. A small number of reports on the preparation of metal oxide thin film materials such as for example iron oxide[11] or ceria nanocomposites[12] by epoxide-assisted gelation can be found in the literature. In the present paper, we present for the first time an epoxide initiated sol–gel route to antimony doped tin oxide TCOs.

Compared to standard alkoxide chemistry, the epoxide method offers a number of advantages for the preparation of TCOs and mixed oxide thin film materials in general. First, this technique utilizes simple metal salts in aqueous solution, typically metal nitrates or halides, eliminating the need for organometallic precursors such as metal alkoxides or the use of an alcohol solvent medium. With an eye on large scale applications the absence of capping agents and alcohol solvents, the use of simple salt precursors and perhaps most importantly the rapid processing times are unique features of this technique. Even without heating of the reagents, the sol formation is almost instantaneous, depending on the amount of epoxide added. The preparation of the deposition solution is normally done at room temperature. Third, the method is in general very well suited for the synthesis of a variety of complex mixed metal oxide materials. Last but not the least, the process allows for improved control over the micro- and nanostructuration of the resulting metal oxide network through modification of the synthesis strategy. When we compare this method to other nonalkoxide based methods, their advantage in the preparation of TCO materials becomes all the more apparent: Chen[13] and Fried et al.[14] reported the synthesis of ATO silica composite and tin oxide coatings respectively by simple solution precipitation using hydroxide as a proton scavenger. This however requires the addition of a stabilizer or capping agent such as oxalate or a surfactant (Pluronic F127) to the sol in order to prevent the precipitation of larger "macroscopic" particulate matter. The addition of stabilizers however negatively impacts the electrical conductivity of ATO thin films after annealing, where it leaves behind a carbonaceous residue. This may be the reason why the above-mentioned research articles do not focus on electrical properties of the so-obtained ATO phases. The preparation of ATO sols from metal salts in absence of capping agents in alcohol solutions are often very time-consuming, as they require working in fairly dilute systems and lengthy refluxing periods of several hours.[15] In some cases, a large fraction of the solvent needs to be removed by evaporation in order to produce a sol viscosity sufficient for thin film deposition.[16] Both, the economic scalability and the materials properties of ATO films speak in favor of the epoxide method. To fully understand the beauty of this system, let us briefly elucidate the reaction mechanism:

Epoxide-Initiated Sol–gel Chemistry. Scheme 1 shows a schematic illustrating the formation of metal hydroxide from metal salt and epoxide which then undergoes polycondensation to yield polymeric or cluster-like polyoxometallates. Temporal and structural evolution of these clusters leads to a colloidal sol of metal oxide nanoparticles. In contrast to alkoxide based chemistries, where the reactive primary metal hydroxides species are created by hydrolysis of metal alkoxide bonds, the epoxide assisted method is initiated by proton abstraction from a water ligand molecule of a partially (or even completely) solvated metal cation $[ML_n(H_2O)_{6-n}]^{+m}$ (see Scheme 1).

Assuming a concerted reaction mechanism for a pure, undoped $SnCl_4$ sol involving for example a chloro-aqua metal cation directly, the epoxide ring is attacked by a nucleophile, namely a "free" uncoordinated corresponding anion of the

Scheme 1. Schematic Showing the Initial Stage (metal monohydroxide formation) of the Epoxide-Assisted Sol–Gel Process[a]

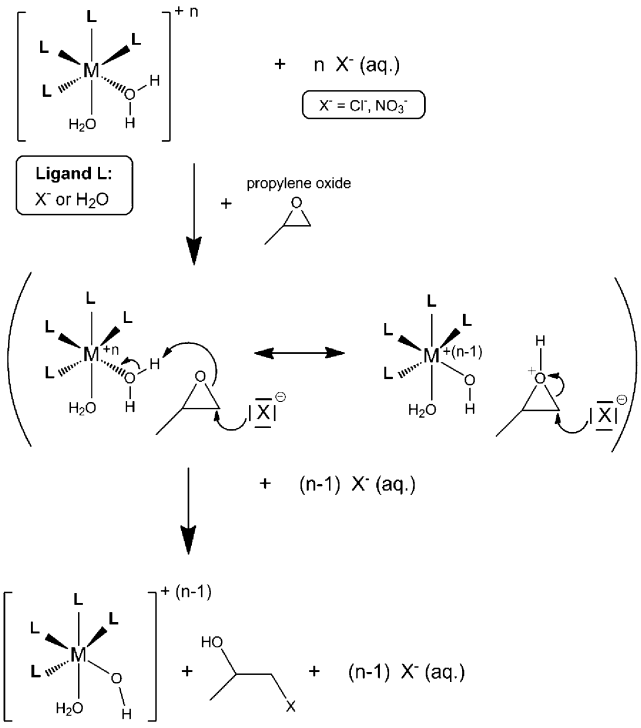

[a]M is a metal ion and X is the counterion of the metal salt.

metal salt X^- (X^- = Cl^-, NO_3^-). As the ring opens, a proton from a water ligand molecule is abstracted. In this way, a single epoxide conversion with $SnCl_4$ yields a mixed chloro-aqua-metal hydroxide of formal oxidation state $(n - 1)$ and a chlorosubstituted alcohol. An alternative and perhaps more relevant mechanism involves first the proton transfer from an acidic water ligand to the epoxide followed by the nucleophilic attack and ring-opening (Scheme 1, center right). The formation of metal oxide network structures requires stoichiometric amounts (typically from 1.2 to 2 mol equiv.) of epoxide per metal ion. Once the metal salt has reacted with one equivalent of epoxide (Scheme 1 and eq 1), a second proton can be abstracted from the chloro-aqua-metal hydroxide resulting in a dihydroxide species according to eq 2. The rate of the proton scavenging reaction strongly depends on the type of epoxide used but also on the acidity of the residual water ligands coordinated to the metal center. Gash et al. reported the gelation times to increase with the epoxide used in the order propylene oxide (PO, C_3H_6O) < trimethylene oxide (TMO, C_3H_6O) < dimethyloxetane (DMO, $C_3H_{10}O$).[8] In addition, the more acidic auqa ions are better proton donors and hence should react preferentially. The acidity of metal transition metal complexes decreases with the ionic radius. Thus, metal cations with a higher oxidation state or formal charge (smaller ionic radii) react faster. Implications of the different water ligand pK_a values will be debated further in the Discussion section.

In this work, PO was used as a sol-initiator reagent. Once added to an aqueous solution containing the chloro-aqua ion $[SnL_4(H_2O)_2]^{4+}$, the chloro-aqua-hydroxo Sn^{4+} complex $[SnL_4(H_2O)OH]^{3+}$ is formed. Because of the intricate nature of the mixed chloro (and nitrato)–aqua complexes, we shall adapt the notation of four unspecified ligands L that are either

Scheme 2. Schematic Illustrating the Various Types of Samples a−c Prepared in This Study along with Their Film Fabrication Process

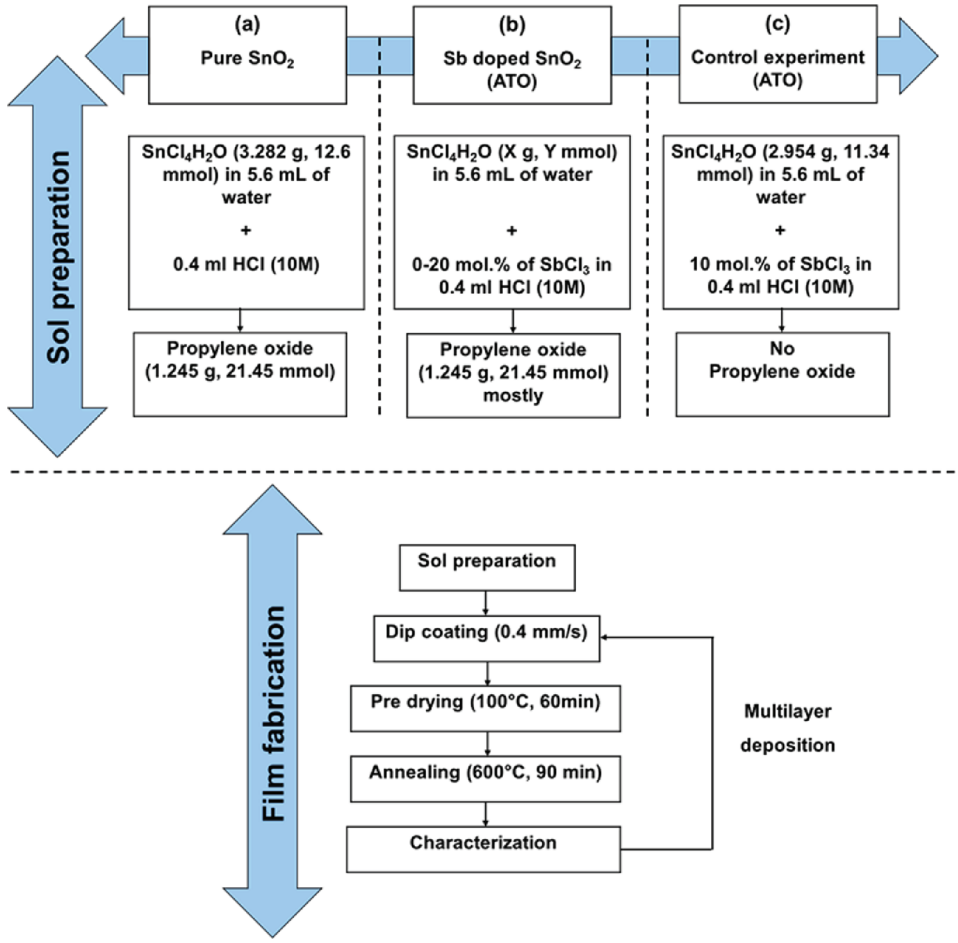

chloride or H_2O when describing the $SnCl_4$ chemistry. The tin hydroxyl complex $[SnL_4(H_2O)OH]$ can undergo olation/oxolation reactions to form condensed tin oxide species. In solution, $SnCl_4$ and the propylene oxide mix together to form a homogeneous solution before a significant increase in pH occurs. The preparation of mixed oxide sols to produce antimony doped tin oxide (ATO) proceeds much in the same way but with both, tin and antimony ions present in solution.

EXPERIMENTAL SECTION

The chemicals used in a typical synthesis were tin tetrachloride hydrate ($SnCl_4{\cdot}H_2O$), antimony trichloride ($SbCl_3$), hydrochloric acid (HCl) and propylene oxide (PO). All reactants were reagent grade quality obtained from Sigma Aldrich and were used as received. Three different types of liquid sols or solutions are discussed in this work: (a) undoped tin oxide sols (b) antimony doped tin oxide (ATO) sols and (c) a liquid solution used as a control experiment, containing both tin and antimony salts but no propylene oxide. Liquid solutions or sols were then deposited onto alkaline free borosilicate glass substrates. Following the deposition process, films were first predried and then annealed to yield the corresponding thin film materials. Of the ATO material (b), multiple layers were deposited as well, in order to achieve larger thicknesses and lower sheet resistance values. Scheme 2 below contains a simplified schematic of the preparation of the various sample groups a, b, and c discussed in this work. It also illustrates film fabrication process of above prepared sols.

In part a, undoped tin oxide films were prepared by dissolving $SnCl_4{\cdot}H_2O$ (3.282 g, 12.6 mmol) in a mixture consisting of 5.6 mL of water and 0.4 mL of 10 M HCl, followed by the slow and dropwise addition of propylene oxide (1.245 g, 21.45 mmol). This mode of addition of PO is preferred because rapid addition results in significant heat evolution given the exothermic nature of the reaction. With rapidly rising temperatures, the kinetics of the sol−gel reaction increase in an uncontrollable manner and quite often a gel is formed. Drop wise addition of the given amounts of chemicals always results in the formation of a stable sol without noticeable warming of the reaction mixture. Further, the viscosity of the solution can be controlled to some extent by the concentration of the propylene oxide in the sol. Generally, up to a certain point of PO addition, the viscosity clearly increases (from 1 cP to about 3−5 cP). Beyond this point, further addition of PO does not result in a markeable increase of the solution viscosity, up to the point, when the sol suddenly begins to gel. The useful range for the deposition of films using this technique is in the "Low-viscosity" (3−5 cP) range. One should be aware of the reactivity and moderate toxicity of epoxide compounds and take appropriate safety precautions. Reactions involving metal salts and epoxides can be quite exothermic and often lead to a rapid warming up of the reaction mixture.

In part b, antimony doped tin oxide sols were prepared by replacing an amount of tin chloride corresponding to a 0−20% molar fraction (doping level) of antimony. The total quantity of Sn and Sb chlorides used always added up to 12.6 mmol. Otherwise the procedure was identical to the one used in a. HCl is added in all preparations a−c because the solubility of $SbCl_3$ in neutral aqueous media is minimal as it almost instantaneously hydrolyses forming antimony oxychloride SbOCl.[17] It is observed, that when antimony chloride was added to tin chloride solutions in dilute HCl, the resulting solution still turns increasingly more turbid (SbOCl precipitation) with higher percentages of antimony present in the mixed sol. However, upon addition of

approximately half of the total amount of PO (~10 mmol), the solution again becomes perfectly transparent, indicating that antimony is going back into solution as it is being consumed by the sol–gel reaction.

Finally, part c is the control experiment used to prove the active role of the expoxide initiator PO in the sol–gel process. A selected mixture of tin and antimony chlorides in dilute HCl was used to deposit a thin film in much the same way as with the previous sols a and b but without addition of PO to the reaction mixture. Note that a higher concentration of hydrochloric acid was needed to keep the Sn and Sb chloride salts soluble. In addition, multiple layers of the two best performing ATO candidates were deposited and characterized separately.

In a typical experiment, a sol was freshly compared according to the selected method (Scheme 2), stirred for 2 min and transferred to the deposition bath. The as-prepared sols have a room-temperature shelf life of several hours (2–5 h) during which the properties of the films do not change noticeably. Precleaned borosilicate glass substrates were dipped in the deposition bath and withdrawn at a speed of 0.4 mm/s from the sol solution exactly 30 min after the addition of the last reagent (PO). A typical dip coating experiment lasts 2.5 min. As deposited films were preannealed at 90 °C for 120 min followed by a 90 min annealing at 600 °C.

The coating thickness was characterized by means of a stylus profilometer. For this purpose, a section of the film was etched with Zn metal/conc. HCl in order to create a step edge suitable for profilometry. The electrical resistivity of the films was determined by a sheet resistance measurement using a standard four-point probe setup. The optical transmission was measured using a UV–visible spectrophotometer. The crystal structure of the films was analyzed by X-ray diffraction (XRD) at grazing incidence (1°) using Cu–Kα radiation. Finally, the surface structure and topography of the coatings was analyzed by means of scanning electron (SEM) and atomic force microscopy (AFM) techniques. The latter provided more precise topographical information about the film roughness.

RESULTS AND DISCUSSION

In the following, we shall discuss the influence of chemical synthesis parameters on the films and their physical properties. The parameter discussion is based on the chemical model of the epoxide assisted gelation described above (Scheme 1).

Film Thickness and Electrical Resistivity. The sheet resistance values of the films were measured on both sides of substrates using the four point probe technique. Measurements were taken at several locations over the entire film and average values calculated. Table 1 shows the variation of the electrical resistivity of the prepared tin oxide films for various Sb dopant levels. One immediately notices, that the pure tin oxide sample a shows no electrical conductivity. With increasing Sb dopant levels from 2.5 to 9.0 at %, the resistivity decreases to its optimum value of around 0.018 Ω cm for a single layer deposition. With further increasing Sb concentration in the sol, the resistivity again increases. Typical film thickness values for (a) undoped and (b) Sb-doped films are on the order of 110–150 nm. The highest antimony loading (20%) resulted in an unusually thin film. The control experiment c shows only a minute film thickness of 22 nm, and the material exhibits no electrical conductivity. This confirms the importance of the epoxide in this type of sol–gel synthesis. In the absence of PO, colloidal particles form much more slowly or not at all, and hence the viscosity of the deposition solution remains much lower, resulting in an extremely thin film.

Table 1. Thickness and Resistivity Values of Films with Various Sb Doping Levels

sample preparation	Sb doping (% mole)	thickness (nm)	resistivity × 10^{-2} (Ω cm)
(a)	0	114	∞
(b)	2.5	118	3.1
(b)	5	154	2.8
(b)	7.5	122	2.1
(b)	9	121	1.8
(b)	10	121	2.9
(b)	12.5	147	4.0
(b)	15	127	3.4
(b)	17.5	116	3.7
(b)	20	72	5.6
(c)	10 (control exp.)	22	∞

Crystalline ATO is an n-type semiconductor material because the addition of the foreign element Sb with 5 valence electrons into the tin oxide matrix introduces additional free electrons to the conduction band. At dopant levels below the optimum value of 9 mol %, the reduction in the resistivity with increasing amounts of Sb is attributed to an increase in the carrier concentration because of the electron donor effect of the dopant. Too high dopant levels, however, have an adverse effect resulting from the sharp rise in the number of trap states arising from too many crystal lattice defects. These traps begin to dominate the carrier concentration above the critical Sb levels, thus resulting in an overall reduction of electron mobility and electrical transport properties.[18] Similar resistivity trends are reported in other works, with the optimum ATO doping concentration in the range 3–14 mol %.[19−23]

Crystallographic Identification. The crystal structure of annealed SnO_2 and ATO films was confirmed by grazing incidence X-ray diffraction (XRD). Figure 1 shows the XRD pattern of an annealed 9 mol % Sb-doped ATO film in red; the reference SnO_2 pattern is given below in black. As expected, the ATO film shows the exact same Bragg reflection signatures which are typical for the cassiterite SnO_2 structure (isostructural with rutile TiO_2). The relative intensities of the various reflections arising from the various crystal plane reflections

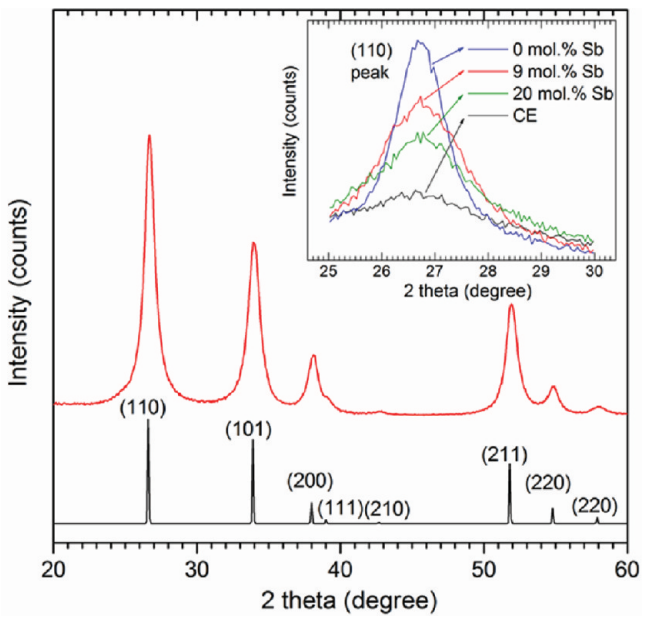

Figure 1. XRD patterns for Sb-doped (9 mol %) SnO_2 layer with the reference SnO2 pattern along with an inset of (110) reflection for different Sb doping levels and control experiment (CE).

(110), (101), (200), (211), (220), etc., also correspond to those of the cassiterite reference. In the inset, the (110) plane reflections of doped and undoped tin oxide and control experiment films are shown. At higher Sb dopant concentrations, the fwhm values of the peak increase and the peak heights decrease gradually which is in fact expected: at very low dopant levels, Sb is incorporated primarily by substitution of Sn atoms in the crystal lattice. With increasing dopant amounts, the incorporation is more likely to occupy interstitial sites which can result in the precipitation of Sb_2O_3 and Sb_2O_5 or antimony oxide enriched nanophases.[24] As a result, films lose their crystallinity with increasing doping concentration and the crystallites become smaller and the peaks wider.

Optical Transmission. Figure 2 shows the optical transmission spectra of the films for selected Sb-doping concentration and of the control experiment. The marked absorption edge at around 320 nm is due to the borosilicate glass substrate UV-cutoff. The highest optical transmittance values (~92%) over the entire visible and into the NIR region of the optical spectrum (400−1400 nm) was observed for undoped and doped (up to 5 mol % Sb) films as well as for the control experiment. Above 5% antimony, the optical quality of the films deteriorates rapidly, particularly in the NIR part of the spectrum (λ > 800 nm). The decrease in the measured optical transmission can be attributed to two main factors, namely (i) the intrinsic absorption of light by interaction with conduction electrons and (ii) scattering losses arising from larger precipitates. During the film preparation, we observe increasing amounts of antimony oxychloride precipitates with increasing dopant levels as discussed in the Experimental Section. Although upon visual inspection of the sol, the antimony seems completely dissolved in the mixture, even at the highest doping levels, it leaves a whitish residue on the as deposited films. This observation is consistent with the sudden loss of optical transmission above 7.5 mol %. We attribute these losses to larger colloidal particles, most probably rich in Sb, which after the deposition form larger aggregates and hence scatter light. Even though scattering losses dominate the film transmittance at higher antimony dopant concentrations, we also note an increasing transmittance loss at very high Sb loadings (>10%) in the NIR region. Aside from the SbOCl precipitate induced scattering, our results are consistent with those of TCO films on glass substrates prepared by spray pyrolysis such as in the works published by Jain and Kumar,[25] Shanthi et al.,[26] and Stjerna et al.[27]

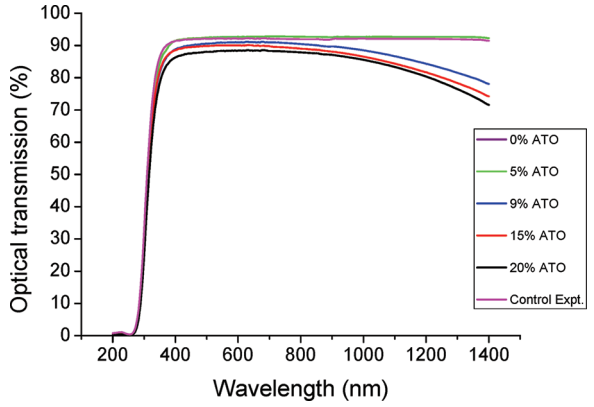

Figure 2. Optical transmittance spectra of the TCOs for various Sb-doping concentrations as well as for the control experiment.

Even though 9 mol % Sb doping yielded the lowest resistivity values in a single deposition ($\rho = 1.8 \times 10^{-2}$ Ω cm), there is a remarkable loss in optical transmission. As indicated by the name TCO, films need to be both transparent and electrically conductive: At 5 mol % Sb doping we find the best compromise between electrical and optical properties with only slightly reduced conductivity $\rho = 2.7 \times 10^{-2}$ Ω cm but perfect transparency. A further decrease in the film resistivity can be achieved by depositing multiple coatings. This part will be explained in detail in the Multilayer Deposition section.

Surface Morphology (SEM, AFM). Figure 3 shows the surface topography (secondary electron SEM images) of undoped and Sb doped SnO_2 thin films. In general, the annealed film structure is influenced significantly by the Sb-dopant level. A network of particles is observed in all the deposited films, including the control experiment (Figure 3a, which refers to a 9 mol % ATO control experiment, where no propylene oxide was added). This type of particle morphology is typical for annealed sol−gel metal oxide coatings. The plain, undoped SnO_2 film exhibits a comparably rough surface with many spherical particle aggregates. They appear quite densely packed and the film shows virtually no surface cracks. This is also confirmed by the AFM analysis shown in Figure 4.

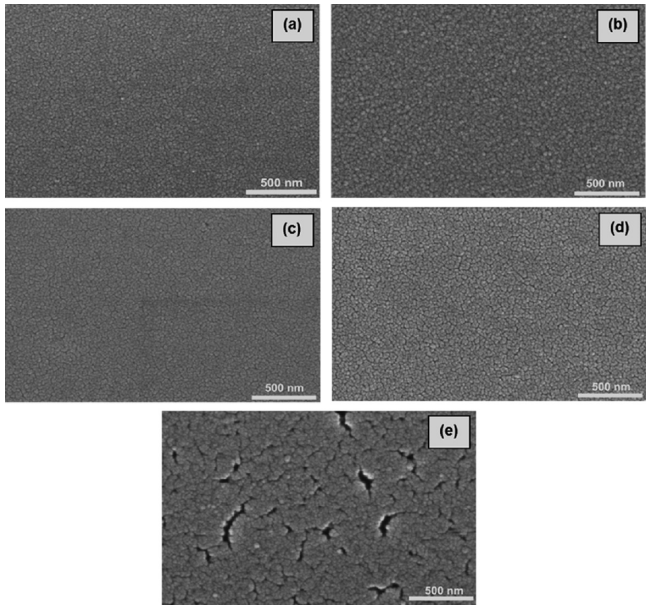

Figure 3. SEM microscopy images of TCO films: (a) 9 mol % ATO control experiment, (b) 0 mol % SnO_2 film, (c) 5 mol % doped ATO, (d) 9 mol % ATO, and (e) 15 mol % ATO.

With the addition of 5 mol % Sb dopant, the film surface smoothens and minute cracks (>20 nm) appear along the particle grain boundaries. The typical domain size of the coherent (crack free) particle aggregate regions is between 50 nm and 100 nm. The same holds for the 9 mol % antimony doped sample in Figure 3d. Because 9 mol % doped ATO produced the highest electrical conductivity, the microstructure of a 9 mol % doped ATO film is shown instead of the 10 mol %. In the case of the 15 mol % doped sample (Figure 3e), the domains become much larger (200−400 nm) and so do the cracks (20−50 nm).

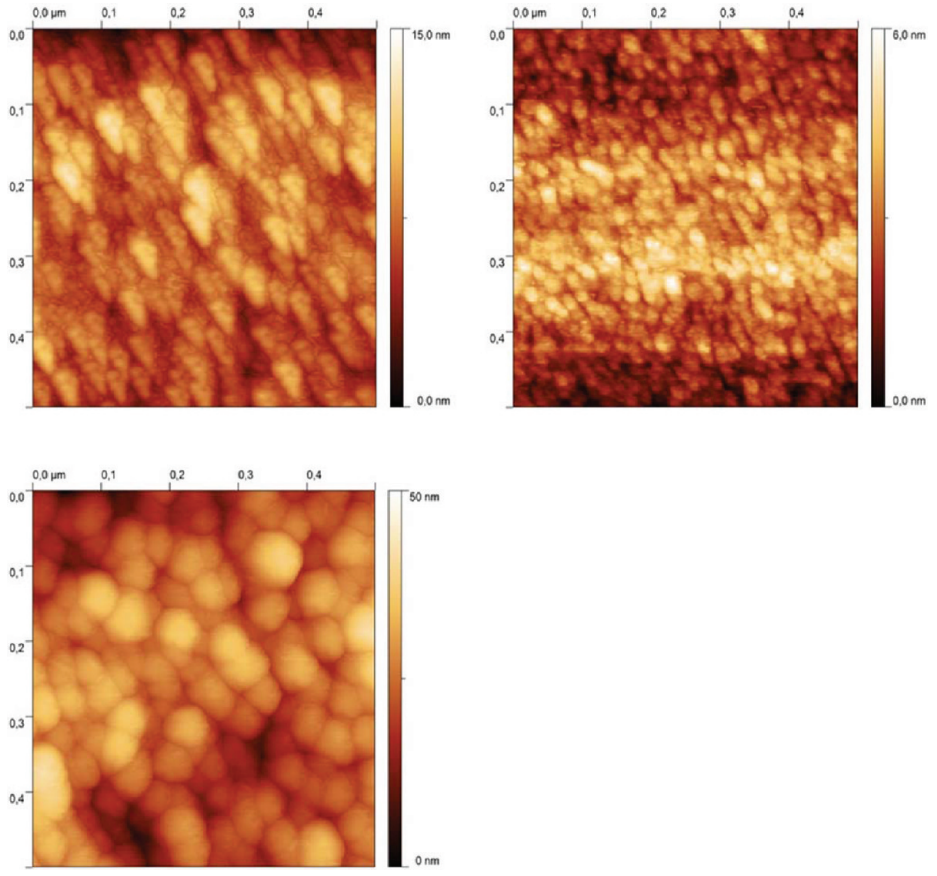

Figure 4. AFM (tapping mode) images of 0% (top left), 5% (top right), and 15% (bottom left) Sb-doped ATO films.

The surface topography in the AFM images in Figure 4 is consistent with the electron microscopy images. Pure SnO_2 films show larger grains up to 50 nm. Their average size is larger than that of a 5% Sb doped film (20−30 nm grain size). A 15% antimony doped material exhibits much larger grains on the order of 60−100 nm. The difference in size may be attributed to the different thermodynamic stability of the respective mixed oxide phases. At the same time, the rms surface roughness decreases from ∼6 to ∼2 nm when going from undoped to 5% Sb doped films. In agreement with the SEM images, the surface roughness of the 15% doped sample is much higher ∼20 nm, and the sample exhibits large cracks which are up to 50 nm deep.

Low Sb dopant levels up to 5% produce smooth films with minimal roughness. Higher Sb concentrations favor larger cracks. The effect of the Sb dopant concentration on the film morphology (grain size and cracking) clearly also reflects in the films physical properties, namely their electrical conductivity and optical transparency. Even though the intrinsic conductivity of Sb doped films should increases to a certain level with the dopant concentration, the higher electrical conductivity of the ATO matrix is to a certain extent offset by an increasing number of structural defects. This explains the relatively weak dependence of the electrical conductivity on the dopant concentration.

Multilayer Deposition. The deposition of thin films from a metal oxide sol requires sufficiently low viscosity of the sol for ease of processing and to yield uniform films. If the viscosity of the sol is too high, gelation may occur and the film thickness will quickly reach several μm. At these thicknesses, film cracking and delamination is almost impossible to control. As a consequence, the practical limit of sol−gel film thicknesses is around 150 nm. In most applications, lower electrical resistivity values than those obtained by a single 100 nm thick layer (on the order of 2 k Ω) are needed. This can be achieved by multiple film depositions. In this work, 1 to 5 layers of the best case candidate films with 5% (best optical transparency vs electrical conductivity) and 9% (lowest total electrical conductivity) were deposited. The experimental procedure was identical to the one used for single layer deposition. After each deposition, the films were annealed at 600 °C for 90 min in air. Multiple deposition experiments without annealing in between each cycle resulted in poor electrical conductivity values. Following the deposition, each coating must be annealed separately in order for the film to develop its electrically conducting properties. Experiments showed the same electrical conductivity (over a larger total film thickness) of single and multiple coatings with final annealing. We believe that the filling of cracks (which are mostly formed during annealing) gives rise to the higher conductivity values, which are observed after a consecutive depositions/annealing procedure. Therefore, it is necessary to anneal in between each cycle of coating.

Film thickness, measured electrical conductivity values, and optical transparency at 600 nm for 1 to 5 layers of 5 and 9% doped ATO films are summarized in Table 2. The film thickness values show a clear trend. The second deposition does not result in a significant thickness increase (less than 30 nm); however, it causes a drastic lowering of the electrical resistivity of more than a factor of 3. It is believed that the

dx.doi.org/10.1021/am300143z | ACS Appl. Mater. Interfaces 2012, 4, 2464−2473

Table 2. Electrical resistivity and total film thickness for multilayer ATO films

	layer no.	thickness (nm)	resistivity × 10^{-2} (Ω cm)
		9 mol % of Sb doping	
1	1	159	3.02
2	2	182	0.91
3	3	275	0.41
4	4	375	0.45
5	5	508	0.50
		5 mol % of Sb doping	
6	1	133	3.05
7	2	142	0.71
8	3	246	0.49
9	4	290	0.49
10	5	498	0.54

second deposition mostly fills residual cracks and voids in the underlying (first) film. In this way, most cracks and other defects are eliminated and the overall connectivity improved, which explains the remarkable increase in the observed electrical conductivity. With each subsequent layer from 3 to 5, the total film thickness increases by roughly the same amount as the original film thickness, namely ∼120 nm. Films with five layers are roughly 0.5 μm in thickness. Interestingly enough, the electrical resistivity decreases strongly from the layer number n from 1 to 2 (by more than a factor of 3) and from 2 to 3 but then reaches a more or less constant value around 5×10^{-3} Ω cm. Our interpretation of these results is that a second layer fills most of the residual cracks of the previously annealed coating and the remainders of film defects are covered by the third layer. After three depositions, the film is of homogeneous quality exhibiting minimal porosity and defects. This explains the more or less constant value of the resistivity after layer number 3. In Tables 1 and 2, two different values of resistivity and film thickness for single coating 9 mol % ATO, has to do with a narrow minimum or "step edge" around 9% Sb. At 10% Sb doping in Table 1, the resistivity is again up to 2.9×10^{-2} Ω cm, which is the pretty much same value as that of a single film in Table 2. The experimental error in the preparation, particularly in the film deposition by dip-coating, clouding of the solution due to precipitation of SbOCl, and redissolution supports this hypothesis.

The optical quality of the films decreases rapidly with increasing number of depositions. As a single layer, the 5% Sb doped films exhibit a significantly higher transmittance than the 9% Sb analogues (see Figure 2). This trend is also confirmed in the multilayer experiments: After 5 deposition cycles, a 5% antimony doped coating still transmits 74% of the light at 550 nm, whereas the 9% doped material is down to only 30%. This is in agreement with the observed single layer transmittance values. For multilayers the transmittance losses are in part codetermined by deposition artifacts. This is evidenced by the fact that transmittance losses do not scale linearly with the film thickness and that they depend very strongly on the Sb dopant concentration.

DISCUSSION

The main goal of this work is to demonstrate the usefulness of epoxide assisted sol−gel chemistry for the preparation of mixed oxide thin film materials. For TCO applications, electrical conductivity (sheet resistance) and optical transparency are the key figures of merit. The overall performance of the film is determined by two main factors, namely, the sol preparation method (the chemistry) and the film deposition and post-treatment.

To better understand this sol−gel method, we first need to understand how chemical parameters affect the sol composition and with that, the final material. Let us therefore have a look at the pure tin oxide sol system a. In general, the formation of colloidal particles is governed by the formation of hydroxide species in solution and their subsequent polycondensation reactions. According to the spectrochemical series which classifies ligands according to their ability to form coordinative bonds with metal d-orbitals, transition metal chloride and nitrate salts in aqueous solution exist in the form of mixed chloro-aqua or nitrato-aqua complexes, respectively. Let us be reminded that water ligands of solvated metal cations are acidic or in other words they act as a source of H^+.

$$[SnL_4(H_2O)_2]^{+4} \rightleftarrows [SnL_4(H_2O)OH]^{+3} + H^+ \quad (1)$$

$$[SnL_4(H_2O)OH]^{+3} \rightleftarrows [SnL_4(OH)_2]^{+2} + H^+ \quad (2)$$

The deprotonation of one or two water ligands from a Sn(IV) cation in solution is shown above in eq 1 and 2. At any given time, the amount of Sn−OH groups in solution is determined by the pK_a of the corresponding water ligand. The pK_a values of HCl and $SnCl_4$ are −7 and −0.6, respectively.[28] The formation of metal−oxygen−metal bonds can be simply viewed as a ligand substitution reaction. Water being a good leaving group, the kinetics of the reaction are primarily determined by the pH and nature of the attacking nucleophile as shown in eq 3.

$$[SnL_4(H_2O)OH]^{+3} + [SnL_4(H_2O)_2]^{+4} \rightleftarrows [(H_2O)L_4Sn - O - SnL_4(H_2O)]^{+6} + H^+ + H_2O \quad (3)$$

The net formation of Sn−O−Sn bonds by olation reaction 3 is favored by higher pH values. Low pH favors the back reaction that is the hydrolysis of Sn−O−Sn bonds. In the same way, a low solution pH causes the protonation of the free OH groups (back reactions of eqs 3 and 4). This explains why plain tin chloride in solution has little propensity to form colloidal particles without a proton sink. This is where the role of the epoxide comes in: The transition state of the expoxide driven sol−gel reaction involves the formation of a protonated epoxide, as shown in Scheme 1 (center right) which competes with the direct concerted and probably less likely reaction mechanism (center left). The attack of the nucleophile on the epoxide leads to an irreversible ring-opening and with that, the proton is consumed irreversibly. So clearly, the epoxide reaction is a stoichiometric not a catalytic process which consumes H^+ from the system and thus is accompanied by an increase in pH as the reaction proceeds. At the same time, with less H^+ left in the system, the formation of hydroxides (according to 1 and 2) and the olation reaction 3 is favored because the reaction product H^+ is continuously removed from the system. In the absence of PO, olation and polycondensation reactions are not favored. Hence no colloidal sol is formed and the viscosity remains low. This explains the low film thickness and the lack of electrical conductivity in the case of the reference sample c.

Now, that we have discussed the pure SnO_2 system, let us turn to the sources of H^+ in the more complex ATO sol (b). At any point in time, the strongest acid left in the system is going to protonate the epoxide first, be that free HCl or the acidic water ligands of the coordinated Sn^{4+} or Sb^{3+} cations,

Scheme 3. Comparison between Epoxide (top) and Standard Alkoxide Chemistries

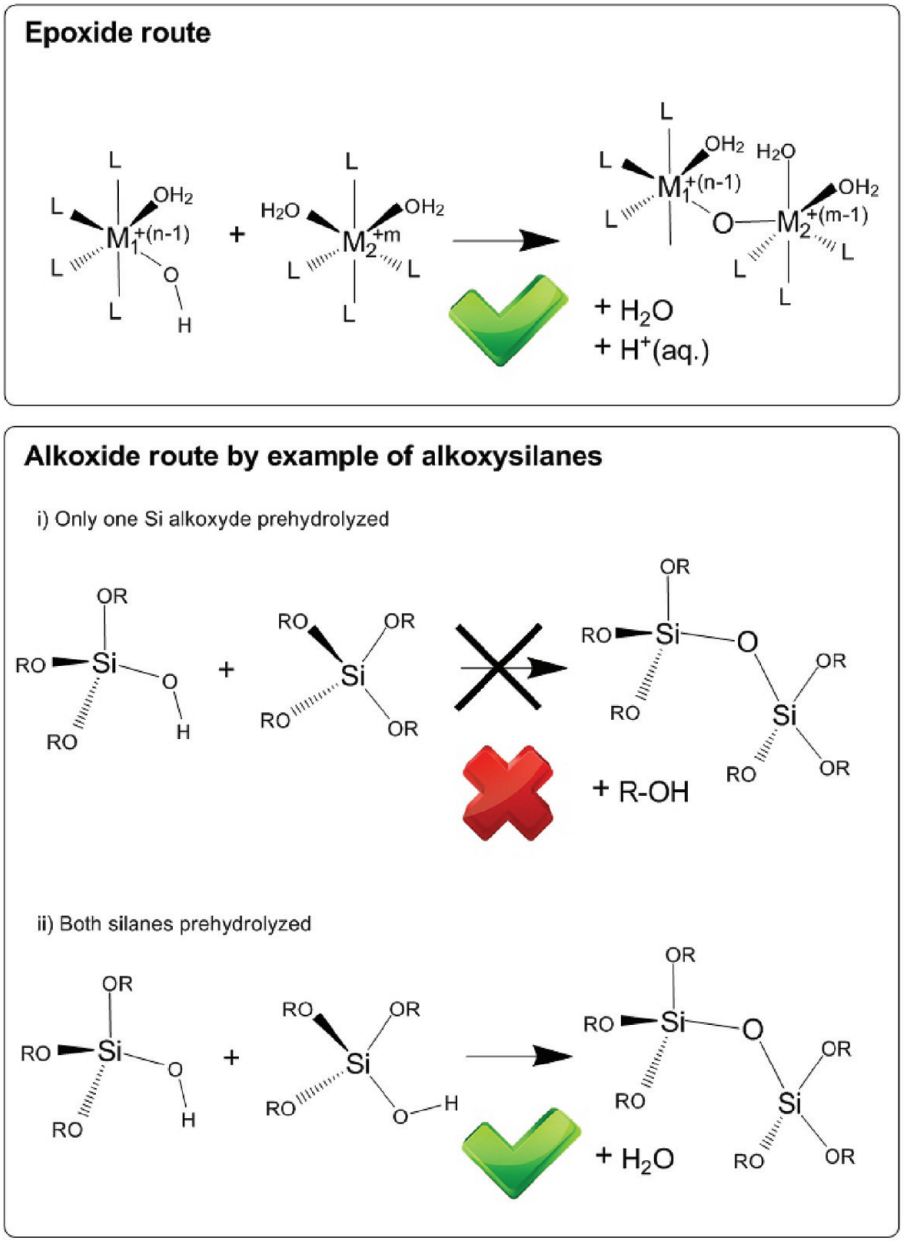

respectively. Let us be reminded that HCl was added to the system in order to keep the $SbCl_3$ soluble. With a pK_a of −7, the former is clearly the strongest acid and therefore will be consumed first. The fact that the reaction mixtures of Sb-doped sols first become turbid (HCl is used up, precipitation of SbOCl occurs) and then discolors again (colloids of Sn and Sb oxides are forming, SbOCl goes back in solution) supports the hypothesis that HCl is indeed consumed first. In a typical synthesis, 21.45 mmol of PO are used. Following the neutralization of HCl, the residual amount of PO (17.45 mmol) is then available to react with $[Sn(H_2O)_6]^{+4}$ and $[Sb(H_2O)_6]^{+3}$ salts. The total amount of Sn and Sb chlorides in any given sol is 12.6 mmol. If the epoxide reacts completely, the average number of hydroxy groups formed per metal center is then 1.38.

In a pure $SnCl_4$ sol (a), the first equivalent of PO is spent on the formation of the monohydroxide according to eq 1. The reaction then proceeds to form the dihydroxide (eq 2). For PO/metal molar ratios >2, the deprotonation of a third water will proceed. Note that the formation of hydroxides by proton abstraction leads to an increase in the pK_a value (loss of acidic character) with increasing number of hydroxide groups formed. As an example, $[Fe(H_2O)_6]^{+3}$ and $[Fe(H_2O)_5OH]^{+2}$ have pK_a values of 2.2 and 3.5, respectively.[29] Note also, that together with the consumption of the propylene oxide, chloride or nitrate anions are irreversibly removed from the system as well (formation of the chloro or nitrato-alcohol product). Thus the ligand shell "L_4" on Sn^{4+} and Sb^{3+} experiences a gradual substitution of chloride and/or nitrate ligands by water, which further complicates the prediction of the true acidity of water ligands.

During the preparation of an ATO sol, once all of the HCl is consumed the aqua ion $[SnL_4(H_2O)_2]^{4+}$ is next to react with PO because it the strongest acid left. We have strong reason to believe that the gradual decrease of acidity of the metal salts

dx.doi.org/10.1021/am300143z | ACS Appl. Mater. Interfaces 2012, 4, 2464−2473

with increasing number of hydroxide and oxide bonds formed additionally influences the process selectivity.

Because of its specific chemical nature, the epoxide process offers improved control over the sol formation, also with respect to the composition and morphology of mixed oxide colloidal systems. But why should this be the case? The answer lies in the weak bonding of Cl^-, NO_3^- and water ligands in the metal coordination shell or in the fact that they are good leaving groups. A pure tin oxide network can start to grow by attack of a single hydroxide species, forming a bridging oxide according to eq 4. Analogously, a Sn−O−Sb bond can be formed through the reaction of a single metal hydroxide with its partner $SbL_3(H_2O)_3^{+3}$, presumably Sn−OH since $SnL_4(H_2O)_2^{+4}$ is the stronger acid, according to eq 4. The attack of the hydroxide M−OH on a second foreign metal center is barely selective.

$$[SnL_4(H_2O)_5OH]^{+3} + [SbL_4(H_2O)_6]^{+4} \rightleftarrows [(H_2O)L_4Sn - O - SbL_4(H_2O)]^{+6} + H^+ + H_2O \quad (4)$$

Therefore, the addition of PO to mixed metal chloride or nitrate solutions should generally lead to homogeneous, amorphous mixed oxide phases whereas standard alkoxide sol−gel methods do not. Scheme 3 explains the crucial difference between the epoxide method (top) and the alkoxide method(bottom) for the formation of mixed oxide colloidal systems. As previously stated, using the epoxide method two metals M_1 and M_2 can form M_1−O−M_2 bonds with relative ease because the water ligands (and chlorides/nitrates) are good leaving groups. In alkoxide sol−gel chemistry, the alkoxide serves as a protecting group and thus R−O− or R−OH are terrible leaving groups.

Let us further elucidate the implications of the leaving group on the formation of mixed metal oxide colloids, by comparing the epoxide assisted reaction mechanism (by example of SnO_2) with standard tetraalkoxysilane sol−gel chemistry: in the latter case, the alkoxyde is a powerful protecting group and thus a direct attack of a silanol group on a second unhydrolyzed tetraalkoxysilane species is virtually impossible as shown in Scheme 3 case i. A reaction only occurs when both Si metal centers have at least one of their OR groups hydrolyzed, such as in case ii. In other words, alkoxyde chemistry requires twice as many hydrolyzed M−OH groups to form metal oxygen metal (M−O−M) bonds where one OH group is the attacking nucleophile and the other takes the role of the leaving group. This has implications for the synthesis of nanocomposite materials such as for example silica/titania mixed oxides. The hydrolysis of Ti-tetraisopropoxide is known to be much faster than that of tetraethoxysilane (TEOS).[30] As a result, alkoxide sol−gel preparation techniques often yield first a colloidal suspension of one oxide (in this case titania) and then a sol of the second compound (silica, or silica doped with traces of residual titania). The formation of mixed oxide colloids by an alkoxide route is infinitely more challenging because of this effect. In comparison, the epoxide route is barely differentiates between metals when forming M−O−M bonds because of the weak bonding of the ligands which surround the central metal cations. As a consequence, an epoxide-assisted approach offers the advantage of increased dispersion and versatility when it comes to the synthesis of multicomponent mixed metal oxide materials.

Aside from the sol formation chemistry, the overall performance of the ATO thin films also relies on optimal deposition and drying techniques. Because of their amorphous (micro- and mesoporous) nature, sol−gel coatings exhibit a certain degree of porosity. This can lead to cracking during drying and annealing treatments, particularly for thicknesses >200 nm per deposition. In this work, the deposition by dip coating and drying/annealing of the films was carried out in a normal laboratory air atmosphere. Our results suggest that the first coating exhibits a significant number of small defects after annealing as evidenced by SEM and AFM microscopy. When a second or even third coating is deposited, the defects in the first layer are filled in with new material, thus releasing the full performance of the ATO material. The defect density on one hand depends on the chemical composition (antimony content) of the sol, but again there is also a certain innate propensity for crack formation of these sol−gel coatings. Optimizations of the deposition and post treatment can lead to a remarkable improvement of the first deposited layer. A detailed investigation of the influence of the deposition method (dip-coating, spin-coating, inkjet deposition) and the post treatment on the final ATO film properties is currently in the making and will be the subject of a follow-up publication.

In the present study on ATO materials, this is further complicated by the reduced solubility of $SbCl_3$ and the precipitation of SbOCl at high antimony dopant concentrations. However, up to 5% Sb, this effect is negligible and we can obtain films of excellent optical quality.

CONCLUSION

The preparation of ATO films by an epoxide-assisted sol−gel method was presented for the first time. The resulting films exhibit electrical resistivity values comparable to ATO films prepared by other liquid chemistry based techniques and the films excel with their outstanding optical transparency values which at low dopant concentrations are virtually identical to that of a plain glass substrate (Figure 2). A multilayer film consisting of 5 subsequent coatings is approximately 0.5 μm thick and has resistance of 100Ω. In contrast to other fabrication techniques, this method uses water as a solvent in combination with very inexpensive raw materials and it is highly versatile. Epoxide-based sol−gel chemistry therefore is a highly promising approach to fabricate virtually any type of metal oxide material. It is easily scalable to large dimensions and offers great promise for future industrial applications in thin films technology such as consumer electronics, photovoltaics and glazing technology.

AUTHOR INFORMATION

Corresponding Author

*E-mail: Matthias.Koebel@empa.ch.

Notes

The authors declare no competing financial interest.

ACKNOWLEDGMENTS

The authors gratefully acknowledge to the Danish ministry of Science for the financial support of this work through the consortium framework “Light-weight, energy-saving materials for the construction industry”. Y.R. acknowledges the support of the Swiss National Science Foundation, Project Nr. PZ00P2_126435/1.

REFERENCES

(1) Walzer, K.; Maennig, B.; Pfeiffer, M.; Leo, K. *Chem. Rev.* **2007**, *107*, 1233.
(2) Suchea, M.; Katsarakis, N.; Christoulakis, S.; Nikolopoulou, S.; Kiriakidis, G. *Sens. Actuators, B* **2006**, *118*, 135.
(3) Wang, N.; Liu, X.; Liu, X. *Adv. Mater.* **2010**, *22*, 2211.
(4) Finley, J. *Thin Solid Films* **1999**, *351*, 264.
(5) Uhlmann, D.; Suratwala, T.; Davidson, K.; Boulton, J.; Teowee, G. *J. Non-Cryst. Solids* **1997**, *218*, 113.
(6) Terrier, C.; Chatelon, J.; Berjoan, R.; Roger, J. *Thin Solid Films* **1995**, *263*, 37.
(7) Minett, M.; Owen, J. *J. Power Sources* **1990**, *32*, 81.
(8) Gash, A.; Satcher, J., Jr.; Simpson, R. *Chem. Mater.* **2003**, *15*, 3268.
(9) Gash, A.; Tillotson, T.; Satcher, J., Jr.; Hrubesh, L.; Simpson, R. *J. Non-Cryst. Solids* **2001**, *285*, 22.
(10) Gash, A.; Tillotson, T.; Satcher, J., Jr.; Poco, J.; Hrubesh, L.; Simpson, R. *Chem. Mater.* **2001**, *13*, 999.
(11) Park, C.; Magana, D.; Stiegman, A. *Chem. Mater.* **2007**, *19*, 677.
(12) Wang, Z.; Pan, Y.; Song, Y.; Cui, H. *J. Sol−Gel Sci. Technol.* **2009**, *50*, 261.
(13) Chen, X. *Mater. Lett.* **2005**, *59*, 1239.
(14) Fried, D.; Ivanova, A.; Müller, V.; Rathousky, J.; Smarsly, B.; Fattakhova-Rolfing, D. *Nanoscale* **2011**, *3*, 1234.
(15) Benrabah, B.; Bouaza, A.; Kadari, A.; Maaref, M. *Superlattices Microstruct.* **2011**, *50*, 591.
(16) Geraldo, V.; Scalvi, L.; Lisboa-Filho, P.; Morilla-Santos, C. *J. Phys. Chem. Solids* **2006**, *67*, 1410.
(17) Theuwissen, A.; Declerck, G. *Thin Solid Films* **1984**, *121*, 109.
(18) Shokr, E. *Semicond. Sci. Technol.* **2000**, *15*, 247.
(19) Terrier, C.; Chatelon, J.; Roger, J. *Thin Solid Films* **1997**, *295*, 95.
(20) Bernardi, M.; Soledade, L.; Santos, I.; Leite, E.; Longo, E.; Varela, J. *Thin Solid Films* **2002**, *405*, 228.
(21) Lee, S.; Park, B. *Thin Solid Films* **2006**, *510*, 154.
(22) Shanthi, S.; Subramanian, C.; Ramasamy, P. *J. Cryst. Growth* **1999**, *197*, 858.
(23) Kim, K.; Lee, S.; Shin, D.; Park, C. *J. Am. Ceram. Soc.* **1994**, *77*, 915.
(24) Jain, G.; Kumar, R. *Opt. Mater.* **2004**, *26*, 27.
(25) Shanthi, E.; Dutta, V.; Banerjee, A.; Chopra, K. *J. Appl. Phys.* **1980**, *51*, 6243.
(26) Stjerna, B.; Olsson, E.; Granqvist, C. *J. Appl. Phys.* **1994**, *76*, 3797.
(27) Richens, D. T. *The Chemistry of Aqua Ions*; Wiley Publishers: New York, 1997.
(28) Bickmore, B.; Tadanier, C.; Rosse, K.; Monn, W.; Eggett, D. *Geochim. Cosmochim. Acta* **2004**, *68*, 2025.
(29) Zhang, X.; Zhang, F.; Chan, K. *Appl. Catal., A* **2005**, *284*, 193.
(30) Patnaik, P. *Handbook of Inorganic Chemicals*; McGraw-hill: New York, 2002.